RSC Advances

ROYAL SOCIETY OF CHEMISTRY

www.rsc.org/advances

A table of contents entry

A facile light-induced synthesis approach was reported for preparing clean-surface PdPt@Pt core-shell nanoparticles with significantly improved electrocatalytic activity.

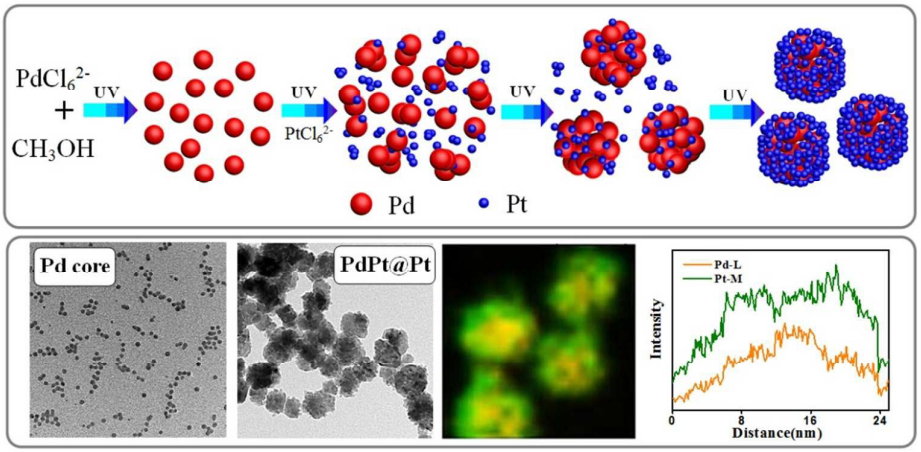

RSC Advances

RSCPublishing

COMMUNICATION

Light-Induced Synthesis of Clean-Surface PdPt@Pt Core-Shell Nanoparticles with Excellent Electrocatalytic Activity

Cite this: DOI: 10.1039/x0xx00000x

Received 00th January 2012,
Accepted 00th January 2012

DOI: 10.1039/x0xx00000x

www.rsc.org/

Tao Wang, Rong Yang, Shenshen Ouyang, Haibo Shi, and Sheng Wang*

We report a facile light-induced synthesis approach for preparing clean-surface PdPt@Pt core-shell nanoparticles. Without using any structure-directing agents, the PdPt@Pt nanoparticles exhibit a clean surface, high porosity and significantly improved electrocatalytic activity for the methanol oxidation reaction (MOR) compared to commercial platinum black, Pt/C and other Pd@Pt materials reported previously.

As fuel cells are considered an energy conversion alternative to traditional fossil fuels, intense development has brought this technology close to pre-commercial viability.[1-4] Until now, platinum (Pt) has been considered as the most effective electrocatalyst.[5-7] However, the sky-rocketing price of Pt in recent years has forced researchers to find efficient ways to enhance the mass activity of a Pt-based catalyst and thus meet the rapidly increasing demands for this multifunctional metal. It is well known that increasing the specific surface area (SSA) is one of the most efficient ways to increase the mass-specific activity.[8] Nanocrystals that possess high SSA such as core-shells structure,[9-11] hollow,[12] dendritic structures[13,14] and even nanocrystals with ultra-small size[15] were fabricated to address this problem. However, the synthesis of such morphologically controlled nanocrystals is limited and generally based on the classical solution-based synthesis method, in which colloidal nanocrystals are synthesised and stabilised in solution with the help of organics or polymers, such as poly(vinylpyrrolidone) (PVP), fatty acids, fatty amine and halide ions. These molecules are often denoted as either surfactants, or structure-directing agents in the literature. However, it was reported that these agents often strongly adsorb and effectively cap the surfaces of metal nanocrystals, blocking the exposure of the surface active sites, and that they are very difficult to remove, leading to a subsequent reduction in catalytic activity.[16-18] It is necessary to develop a chemical synthesis protocol free of structure-directing agents for the production of electrocatalysts for further improvement of the catalytic reactivity.

In this study, we attempted to address these problems by producing PdPt@Pt core-shell nanoparticles via a simple light-induced synthetic approach using methanol as a reducing agent. Without the aid of any structure-directing agents, the core-shell nanoparticles exhibited a clean surface and high porosity. These nanoparticles also exhibited excellent electrocatalytic activity that is 10.5 times and 6.4 times higher than those of commercial Pt black and Pt/C catalysts for the MOR in acidic medium. The methodology developed in this work represents a new opportunity for exploring clean-surface, high-performance metal nanocrystals with diverse potential applications.

The PdPt@Pt core-shell nanoparticles were synthesised using a two-step light-induced approach. According to investigations of nanoparticles photoinduced by UV illumination, UV light acts as an energy trigger that can excite noble metal precursors to form activated species, which in turn react with methanol.[19,20] All of the reactions were performed in a photoreaction instrument with a controlled light intensity (S1, S2, S10). Initially, Pd seed nanoparticles were first photoreduced in a Pyrex glass tube under UV illumination. Then, after injecting Pt precursor into the Pyrex glass tube, Pt shell nanoparticles were photoreduced. Finally, via the aggregation tendency of nanoparticles, the final core/shell nanostructures were achieved.

To prepare PdPt@Pt NPs, Pd seed nanoparticles were first synthesised. We synthesised uniform, spherical Pd seed nanoparticles by reducing Na_2PdCl_4 with methanol in an aqueous solution under UV illumination for 5 h. A transmission electron microscopy (TEM) image of prepared Pd seeds with average size of 3 nm is shown in Fig. 1a. A high resolution TEM (HRTEM) image of a single Pd seed and the corresponding fast Fourier-transform (FFT) pattern indicate that the Pd nanoparticle possessed a single-crystalline structure (Fig. 1b). The d spacing between adjacent lattice fringes (2.23 Å) is very close to that of the {111} planes of face-centred cubic (fcc) Pd (2.25 Å).

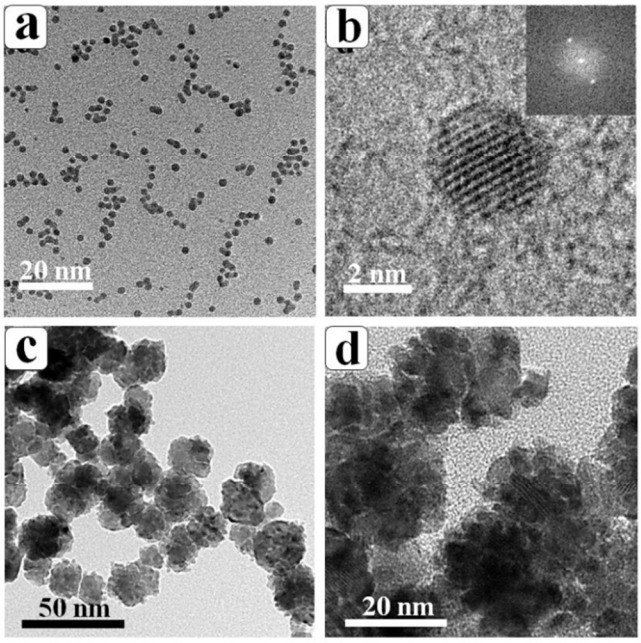

Fig. 1. (a) TEM image of Pd seed nanoparticles synthesised using a light-induced approach. (b) HRTEM image of a single Pd seed nanoparticle and the corresponding FFT pattern (inset). (c) Typical TEM image of PdPt@Pt core-shell nanoparticles synthesised using a light-induced approach in the presence of Pd seeds in a methanol/H_2O solution. (d) Higher-magnification TEM images of the sample.

Next, the spherical Pd nanoparticles were used as seeds for the subsequent production of PdPt@Pt nanoparticles. H_2PtCl_6 was used as the Pt precursor and injected into the reaction tube, which contained a mixture of Pd seed nanoparticles and methanol solution. Upon UV illumination, PdPt@Pt core-shell nanoparticles were successfully obtained. Fig. 1c and 1d show TEM images of the obtained nanoparticles synthesised at a Pd precursor to Pt precursor molar ratio of 1:2. The product was found to consist of well-dispersed spherical nanoparticles. The average diameter of the nanoparticles was approximately 20 nm. To further study the nanoparticles, HRTEM was used to characterise an individual particle (Fig. 1d). The image shows that the prepared product consisted of many smaller nanoparticles, clearly demonstrating the porosity of the nanoparticles.

A high-angle annular dark field scanning TEM (HAADF-STEM) image, and selected-area element analysis maps of Pd (orange) and Pt (green) atoms are shown in Fig. 2. For an individual nanoparticle, although the distribution of two atoms could be observed throughout the entire area, the representative area of Pt atoms was larger than that of Pd atoms. Upon further survey of the two element analysis maps, it can be confirmed that Pd was mainly concentrated in the particle centre, whereas Pt was mainly concentrated at the outer edge of the nanoparticle, indicating the formation of a PdPt@Pt core-shell structure (core rich in Pd and shell rich in Pt). The energy-dispersive X-ray spectroscopy (EDX) mapping profile is shown in S5, from which the Pd:Pt atomic ratio was determined to be 37:63. This result is in agreement with the result obtained from inductively coupled plasma-atomic emission spectrometry (ICP-OES) analysis (Pd:Pt = 34.8:65.2). This ratio is identical to that of the feeding molar ratio of 1:2 Pd:Pt. That is, the PdPt@Pt nanoparticles were formed without loss of metal precursors.

Fig. 2b shows a typical HRTEM image of an individual PdPt@Pt core-shell nanoparticle, and reveals that the PdPt@Pt nanoparticle was a single crystal with high crystallinity, as confirmed by the corresponding FFT pattern (inset of Fig. 2b). The observed lattice fringes were coherently extended over the entire nanoparticle. These observed fringes, with a spacing of 2.28 Å, are in agreement with a (111) plane spacing of fcc Pt. No obvious grain boundary was observed between Pt and Pd because of the extremely high lattice match between Pt and Pd (99.23%). The wide-angle XRD profile of the PdPt@Pt nanoparticle was also assigned to (111), (200), (220), (311), and (222) diffractions of a single-phase fcc crystal structure (S3), which is consistent with the FFT pattern. All of these results show that, even though the core and shell were compositionally different, the crystallographic structure was uniform and coherent over the entire nanoparticle.

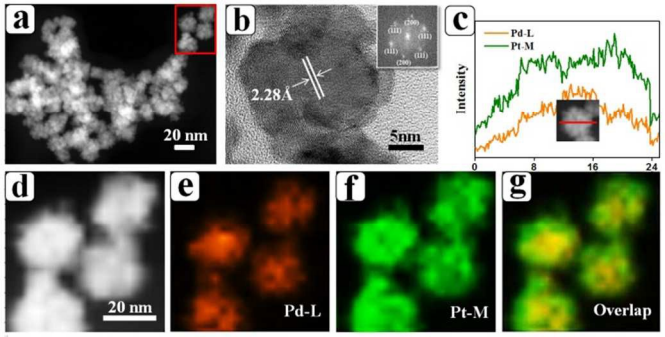

Fig. 2. (a) Dark-field TEM images of PdPt@Pt core-shell nanoparticles. (b) High magnification TEM image of a single PdPt@Pt core-shell nanoparticle and the corresponding FFT pattern (inset). (c-g) HAADF-STEM-EDS mapping images and line scanning profiles of the PdPt@Pt core-shell nanoparticles.

An N_2 adsorption–desorption isotherm of the PdPt@Pt core-shell nanostructures revealed a large surface area of 24.6 $m^2 g^{-1}$ (S4). The pore-size distribution was further investigated, which gives a random distribution of pore sizes ranging from 1 to 20 nm, corresponding to the porous structures of the densely packed core-shell nanoparticles observed in the TEM images (Fig. 1d). The combination of a high surface area with a porous nanoarchitecture (supplying a great number of edges and absorption sites) is advantageous for catalytic applications.

Fig. 3a and 3b show the results of X-ray photoelectron spectroscopy (XPS) analysis of the Pt 4f and Pd 3d spectra for the Pd@Pt core-shell nanoparticles. As shown in Fig. 3a, Pt 4f can be divided into 71.2 eV (Pt $4f_{7/2}$) and 74.5 eV (Pt $4f_{5/2}$), which are assigned to Pt^0 species, and 72.8 eV (Pt $4f_{7/2}$) and 76.1 eV (Pt $4f_{5/2}$), which are assigned to Pt^{II} species.[21,22] Interestingly, in the Pd 3d spectra (Fig. 3b), there are three distinct sets of Lorentzian curves. The two sets of curves included peaks at 335.7 eV (Pd $3d_{5/2}$) and 341.0 eV (Pd $3d_{3/2}$), which are attributed to Pd^0 species; and 337.6 eV (Pd $3d_{5/2}$) and 342.9 eV (Pd $3d_{3/2}$), which are attributed to Pd^{II} species.[21,22] Adjacent to the Pd $3d_{5/2}$ signal, there is a shoulder peak at 331.9 eV with a strong intensity that is rarely observed in most studies of Pt-Pd bimetallic nanocrystals. According to previous reports, this peak should be attributed to the core-level spectrum for Pt $4d_{3/2}$ as the peak intensity far exceeds that of Pd.[23,24] Considering that XPS is a surface-sensitive quantitative spectroscopic technique that measures the elemental composition from a depth of 0 to 10 nm

in a material, X-ray beams must first pass through the shell material before they can reach the core material. This mechanism caused the signal of the shell element (Pt) to be significantly stronger than that of the core, which helped to further demonstrate the core-shell structure of the synthesised nanoparticles.

Based on the integrated area and sensitivity factors of Pd 3d and Pt 4f, the surface ratio of Pd and Pt atoms was calculated to be 5.8:94.2 (S5), which indicates a large discrepancy with the atomic ratio determined by EDX and ICP-AES. This discrepancy suggests that the particle surface was significantly rich in Pt. Combined with the elemental mapping results, these findings strongly support the notion that the PdPt@Pt nanoparticles possess a core–shell structure.

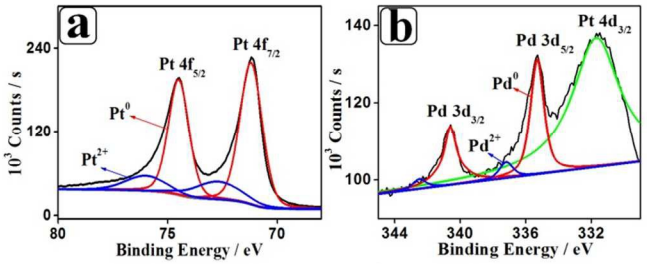

Fig. 3. (a) Pt 4f and (b) Pd 3d XPS spectra of the PdPt@Pt core-shell nanoparticles.

To elucidate the morphological evolution of the PdPt@Pt core-shell nanoparticles, their formation progress was investigated using a time sequential evolution experiment. For comparison, the morphological evolution of pure Pd and Pt nanostructures was first studied individually under identical experimental conditions. TEM images and UV/vis spectroscopic analysis of the growth process of Pd revealed the slow reduction of the Pd precursor. Over a long period of reduction (0 h to 5 h), the sample mainly consisted of monodispersed Pd nanoparticles with high crystallinity. As time elapsed, slight aggregation was observed (6 h to 7 h) (S6). Conversely, the reduction of Pt was rather quick, as small Pt particles of approximately 2 nm formed within 1 h. As the reaction time reached 2 h, the individual Pt nanoparticles began to aggregate into larger particles. From 3 to 4 h, a monodispersed nanoflower morphology evolved (S7). Although the reduction rates were rather different, both pure Pt and Pd exhibited a natural tendency to grow into aggregated structures in this synthetic system and both exhibited single crystalline structures. Some studies have shown that small particles exhibit a high surface free energy because of their large surface area-to-volume ratio and have a tendency to attach to adjacent particles to reduce their surface energy.[25-27] Therefore, it is reasonable that the growth mechanism of both pure Pt and Pd nanoparticles is an oriented attachment mechanism.[28-30]

Fig. 4 presents TEM images of PdPt@Pt core-shell nanoparticles collected periodically throughout the entire reaction. When the reaction mixture was illuminated by UV light for 1 h, the obtained product was a mixture of nanoparticles and small aggregates. When the reaction time was increased to 2 h, a large number of branched structures of different sizes began to appear, which were considered to be the aggregates of many small nanoparticles. In addition, the individual nanoparticles could be observed at the same time. After 3 h, the structure changed from the branched morphology to a spherical morphology, with dozens of small nanoparticles interconnected to form a porous network. Denser spherical structures were observed up until 4 h of illumination, and these structures could maintain their morphology for at least 1 h. Considering the single crystalline nature of the final products (Fig. 2b, S8), the growth mechanism of the PdPt@Pt core-shell nanoparticles is described as an oriented attachment mechanism, similar to that of its parent metals. From the energy view point, aggregation between the particles takes place, provided if aggregating particles possess high surface energy. When Pt nanoparticles formed, there should be Pt-Pt and Pd-Pd (already aggregated) that existed as the predominant component in the solution. Then, the Pt-Pt and Pd-Pd aggregated to reduce surface-interface energy, which made the whole system energy further decrease. Finally, with complete consumption of Pd, and continuous formation of Pt, excessive Pt nanoparticles aggregated around the aggregation to form the final product. The growth process can be rationalized by the scheme shown in Fig. 5.

Because aggregation is a spontaneous process that decreases the total surface free energy of a system; thus, it cannot be prevented. For a clean system without any stabilizer, small size nanoparticles may be unstable at such light intensity, whereas large nanoparticles can withstand it for a period of time. From the TEM images, PdPt@Pt NPs could be observed gradually from 3 h to 4 h. When the reaction time lasted for 5 h, the morphology remained unchanged. From 5 h to 6 h, some aggregation could be observed (S9).

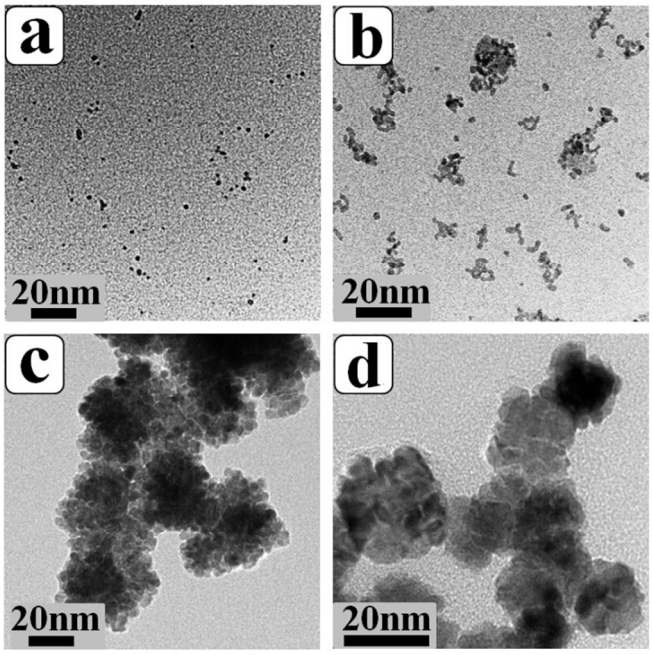

Fig. 4. TEM images of PdPt@Pt core-shell nanoparticles collected at different growth stages: (a) 1, (b) 2, (c) 3, and (d) 4 h.

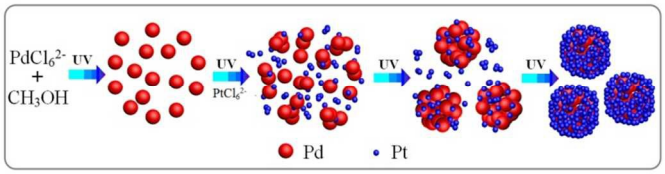

Fig. 5. Schematic illustration of the formation mechanism of the PdPt@Pt core-shell nanoparticles.

Inspired by their attractive properties, we tested PdPt@Pt as an electrocatalyst for the MOR. For comparison, commercial Pt black, Pt/C catalysts, and pure Pt nanoflowers obtained under the same reaction conditions (the sample in S11) were analysed under the same conditions. As shown in Fig. 6a, the ECSA of the PdPt@Pt core-shell nanoparticles was far greater than those of the reference samples. It is well known that the electrocatalytic activity of the catalyst can be assessed by two important parameters, *i.e.*, current density and onset potential.[31] The mass normalised current density of PdPt@Pt in the positive sweep was 2.72 times, 6.37 times and 10.51 times higher than those of the pure Pt nanoflowers, Pt/C and Pt black, respectively (Fig. 6b). In addition, a remarkable negative shift of the onset potential was also observed in comparison with Pt/C (ca. 20 mV), Pt nanoflowers (ca. 70 mV) and Pt black (ca. 140 mV), which resulted in a large enhancement in electrocatalytic activity at low potential. To further evaluate the stability of PdPt@Pt core-shell nanoparticles, chronoamperometric experiments were conducted for 3600 s (Fig. 6c). PdPt@Pt possessed excellent stability during the entire time range. Such a significant enhancement in electrocatalytic activity may be explained by the following observations. First, the electroactivity normalised by the surface area of the PdPt@Pt suggests that the porous structure of PdPt@Pt can provide abundant active sites including defect sites and step edges, thus enhancing the dissociation of water and methanol molecules.[32,33] Additionally, both the negative shift of the onset potentials and the catalyst stability confirm that highly miscible Pd atoms in the Pd-riched core coherently match the lattice structure of the exterior Pt-riched shell, which leads to the formation of the inserted pseudo Pt-Pd alloy heterointerface. Pd (as an oxophilic element) can enhance the removal of adsorbed CO on neighbouring Pt atoms by adsorbing oxygen-containing species.[10,34]

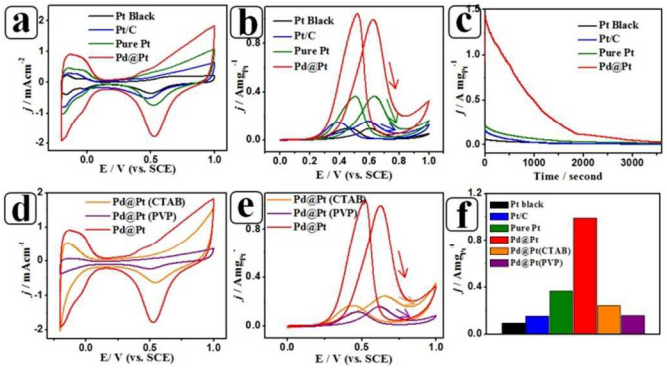

Fig. 6. Comparison of the electrocatalytic properties of the samples: (a) CV curves recorded in 0.5 M $HClO_4$ solutions with a scan rate of 50 mV/s, (b) mass activity, and (c) stability (at 0.5 V). Comparison of the electrocatalytic properties of the clean-surface, CTAB- and PVP- adsorbed PdPt@Pt nanoparticles (d) in 0.5 M $HClO_4$ solution, (e) mass activity. (f) Graphical comparison of mass activities of all catalysts in acidic media. Mass activities are given as kinetic current densities (*j*) normalised with the loading amount of Pt. In (a) and (d), current densities were normalised with reference to the geometric area of a working electrode (0.03). The MOR was recorded in 0.5 M $HClO_4$ + 0.5 M CH_3OH solution at a scan rate of 50 mV/s.

The effects of structure-directing agents were investigated by applying two common structure-directing agents, CTAB and PVP. The electrochemical properties of the clean-surface and PVP/CTAB-adsorbed PdPt@Pt core-shell nanoparticles are shown in Fig. 6d and 6e. It is obvious that the ECSA significantly decreased after structure-directing agent adsorption. According to the calculations, the ECSAs of the PVP- and CTAB-adsorbed PdPt@Pt nanoparticles were 7.1 and 17.3 m^2g^{-1}, that is, 6.1 and 14.8% of the clean-surface ECSA, respectively. PVP has the greatest impact on the ECSA. Additionally, the electrocatalytic activity is inhibited largely due to the reduction in the ECSA for the MOR. It was found that PVP exhibited the greatest reduction in mass activity, with approximately 85.1% of the mass activity lost after PVP-adsorption. Similarly, approximately 75.6% mass activity was lost for CTAB-adsorbed nanoparticles compared with that of the clean-surface PdPt@Pt nanoparticles. It was reported that the adsorption energies for CTAB and PVP adsorbed on the (111) facets of Pt are 5.5 and 24.6 eV, respectively, which indicates that PVP possesses a greater adsorption capacity and inhibition than CTAB.[16] This finding is in agreement with our results.

The excellent performance of the MOR by the PdPt@Pt core-shell nanoparticles was further evaluated by comparing this result with those of other PdPt@Pt samples reported recently, and the corresponding results are presented in Table S3 (S12). The effect of structure-directing agents is much greater than the size/structure effect on the electrocatalytic performance. Because the effect of structure-directing agents on the electrocatalytic performance affects the inhabitation of active sites on the molecular level, these agents are like "organic armour" covering the active sites and blocking reactants from approaching the metal surface, no matter how many active sites or special structures the nanocrystals have. Furthermore, among the reaction systems that did not use a structure-directing agent, our clean-surface PdPt@Pt sample still shows the best electrocatalytic performance. This result is attributed to the high purity of our photoreduction system, in which there was no organic reactant other than methanol.

In conclusion, we developed a light-induced synthesis approach for preparing porous clean-surface PdPt@Pt core-shell nanoparticles. Due to the synergism between Pt and Pd, porous structures and clean-surfaces, the PdPt@Pt core-shell nanostructures exhibited excellent electrocatalytic performance for the MOR. The proposed method provides a novel pathway for the synthesis of metal nanocrystals with clean surface and porous structures suitable for electrocatalysis and other applications.

This work was supported by NSFC (51471153, 31070888, 21103152 and 51372227), ZJNSF (R2101054, LY14E020011), ZJLTSTI (2011R50003), ZJWTARP (2012C23050) and 521 Talent Project of ZSTU.

Notes and references

Address: Key Laboratory of Advanced Textile Materials and Manufacturing Technology, Ministry of Education, Zhejiang Sci-Tech University, Hangzhou 310018, P. R. China. E-mail: wangsheng571@hotmail.com; Fax: +86 571 86843624; Tel: +86 571 86843624

† Electronic Supplementary Information (ESI) available: Experiment details, formation mechanism of noble metal nanoparticles under UV light irradiation, XRD data, N_2 adsorption-desorption isotherm, TEM images of formation progress for Pt and Pd, other data. See DOI: 10.1039/c000000x/

1 *Handbook of Fuel Cells: Fundamentals, Technology and Applications*, ed. W. Vielstich, A. Lamm and H. Gasteiger, Wiley, Chichester, UK, 2003.

2 M. S. Dresselhaus and I. L. Thomas, *Nature*, 2001, **414**, 332-337.
3 F. Y. Cheng and J. Chen, *Chem. Soc. Rev.*, 2012, **41**, 2172-2192.
4 F. Achmad, S. K. Kamarudin, W. R. W. Daud and E. H. Majlan, *Applied Energy*, 2011, **88**, 1681-1689.
5 J. Chen, B. Lim, E. Lee and Y. Xia, *Nano Today*, 2009, **4**, 81-95.
6 J. Wu and H. Yang, *Acc. Chem. Res.*, 2013, **46**, 1848-1857.
7 W. Yu, M. D. Porosoff and J. G. Chen, *Chem. Rev.*, 2012, **112**, 5780-5817.
8 J. Gu, Y. W. Zhang and F. Tao, *Chem. Soc. Rev.*, 2012, **41**, 8050-8065.
9 H. Wu, H. Li, Y. Zhai, X. Xu, and Y. Jin, Adv. Mater., 2012, **24**, 1594-1597.
10 H. Ataee-Esfahani, M. Imura and Y. Yamauchi, *Angew. Chem.,* 2013, **125**, 13856-13860.
11 N. V. Long, Y. Yang, C. M. Thi, N. V. Minh, Y. Cao, M. Nogami, *Nano Energy*, 2013, **2**, 636-676.
12 L. Wang and Y. Yamauchi. *J. Am. Chem. Soc.*, 2013, **135**, 16762-16765.
13 B. Lim, M. Jiang, P-H. C. Camargo, E. C. Cho, J. Tao, X. Lu, Y. Zhu and Y. Xia, Science, 2009, **324**, 1302-1305.
14 W. Liu, P. Rodriguez, L. Borchardt, A. Foelske, J. Yuan, A-K. Herrmann, D. Geiger, Z. Zheng, S. Kaskel, N. Gaponik, R. Kötz, T. J. Schmidt, A. Eychmüller, *Angew. Chem. Int. Ed.* 2013, **52**, 9849 – 9852.
15 F. Saleem, Z. Zhang, B. Xu, X. Xu, P. He, X. Wang, *J. Am. Chem. Soc.*, 2013, **135**, 18304−18307.
16 S. Wang, L. Kuai, Y. Huang, X. Yu, Y. Liu, Li, W. L. Chen and B. Geng, *Chem. Eur. J.*, 2013, **19**, 240-248.
17 C-H. Cui and S-H. Yu, *Acc. Chem. Res.*, 2013, **46**, 1427-1437.
18 Z. Nu and Y. Li, *Chem. Mater.*, 2014, **26**, 72−83.
19 M. Harada and H. Einaga, *Langmuir*, 2006, **22**, 2371-2377.
20 M. Sakamoto, M. Fujistuka, T. Majima, *J. Photoch. Photobio. C.*, 2009, **10**, 33-56.
21 W. Liu, P. Rodriguez, L. Borchardt, A. Foelske, J. Yuan, A-K. Herrmann, D. Geiger, Z. Zheng, S. Kaskel, N. Gaponik, R. Kötz, T. J. Schmidt and A. Eychmüller, *Angew. Chem. Int. Ed.*, 2013, **52**, 9849 -9852.
22 K. Yamamoto, T. Imaoka, W. J. Chun, O. Enoki, H. Katoh, M. Takenaga and A. Sonoi, *Nat. Chem.*, 2009, **1**, 397-402.
23 B. Veisz, L. Tóth, D. Teschner, Z. Paál, N. Győrffy, U. Wild and R. Schlögl, *J. Mol. Catal. A*, 2005, **238**, 56-62.
24 B. I. Boyanov and T. I. Morrison, *J. Phys. Chem.*, 1996, **100**, 16318-16326.
25 B. Lim and Y. Xia, *Angew. Chem., Int. Ed.*, 2011, **50**, 76-85.
26 B. Lim, M. Jiang, T. Yu, P. C. Camargo and Y. Xia, *Nano Res.*, 2010, **3**, 69-80.
27 A. Halder, N. Ravishankar, *Adv. Mater.*, 2007, **19**, 1854-1858.
28 J. F. Banfield, S. A. Welch, H. Zhang, T. T. Ebert and R. L. Penn, *Science*, 2000, **289**, 751-754.
29 H-G. Liao, L. Cui, S. Whitelam and H. Zheng, *Science*, 2012, **336**, 1011-1014.
30 D. Li, M. Nielsen, J. I. Lee, C. Frandsen, J. Banfield and J. D. Yoreo, *Science*, 2012, **336**, 1014-1018.
31 B. A. Kakade, T. Tamaki, H. Ohashi and T. Yamaguchi, *J. Phys. Chem. C*, 2012, **116**, 7464-7470.
32 N. Tian, Z. Zhou, S. Sun, Y. Ding and Z. Wang, *Science*, 2007, **316**, 731-735.
33 Z. Zhou, Z. Huang, D. Chen, Q.Wang, N. Tian and S. Sun, *Angew. Chem.*, 2010, **122**, 421-424.
34 Y. Liu, M. Chi, V. Mazumder, K. L. More, S. Soled, J. D. Henao, S. Sun, *Chem. Mater*., 2011, **23**, 4199-4203.